J. Phys. B: At. Mol. Opt. Phys. **46** (2013) 215002 (9pp) doi:10.1088/0953-4075/46/21/215002

Complete Auger decay pathways of Kr $3d^{-1}$ hole levels including direct double processes

J L Zeng, P F Liu, W J Xiang and J M Yuan

Department of Physics, College of Science, National University of Defense Technology, Changsha Hunan, 410073, People's Republic of China

E-mail: jiaolongzeng@hotmail.com

Received 5 August 2013, in final form 27 September 2013
Published 28 October 2013
Online at stacks.iop.org/JPhysB/46/215002

Abstract

The detailed level-to-level single and double Auger decay rates of Kr $3d^{-1}$ hole states are investigated in the framework of the first and second perturbation theory implemented by distorted wave approximation with the balanced large-scale configuration interaction of the successive ions being taken into account. The branching ratios of cascade and direct double Auger decay to the total probability are predicted to be 16.5% and 16.1%, respectively, for Kr $3d^{-1}_{5/2}$ and 16.8% and 17.2% for Kr $3d^{-1}_{3/2}$, resulting in total double branching ratios of 32.6% and 34.0% for the two levels of Kr $3d^{-1}$ hole. A comparison is made with the available experimental results on the branching ratio into triply charged ions and good agreement was found with the most recent published work. This work represents the first theoretical study to correctly explain the experimental measurements. The complete pathways were depicted by including the direct double Auger decay process. Compared with the Auger decay of Ar $2p^{-1}$, the fraction of the cascade double of Kr $3d^{-1}$ is dramatically enhanced yet that of direct double Auger processes is only slightly increased.

1. Introduction

Core-shell photoionization is an efficient way to investigate atoms, molecules, clusters and solid state matters, as both the photoelectrons ejected from the core hole and the subsequent emitted electrons carry information on the target. With the advent of extreme ultraviolet [1] and x-ray [2] free-electron lasers, it is easy to experimentally produce such core hole states in the interaction of (soft) x-rays with atoms [3, 4]. After the production of an inner-shell vacancy, an Auger process follows with the nonradiative rearrangement of the electronic structure of atoms. Usually it leads to emission of one of the outer electrons in filling the vacancy, which is referred to as a single Auger decay (SAD) process. If two electrons were emitted sequentially or simultaneously in the decay process, it is called a cascade or direct double Auger decay (CDAD or DDAD). The DDAD process involves electron correlations to a higher degree than the SAD process, as it is forbidden in the physical picture of the independent electron model. It is usually assumed to be a weak process, yet it has nontrivial effects on the x-ray interaction with atoms [5]. Its study is both interesting as well as challenging from a fundamental viewpoint.

Extensive experimental investigations have been carried out for Auger decay, including the double Auger decay (DAD) process, over the past several decades. With the development of experimental technology, various coincidence measurement techniques have been utilized to observe the Auger decay of the inner-shell vacancy of rare gases (for examples see [6–9]). By means of photoelectron-ion coincidence spectroscopy, Brunken *et al* [10] investigated the decay of shallow inner-shell hole states of noble gases including Kr $3d^{-1}$ to disentangle different contributions to the electron spectrum and to determine the probability of the final ionic charge states. By using a multielectron coincidence method, Palaudoux *et al* [11] and Andersson *et al* [12] experimentally investigated the decay pathways including the double Auger process of Kr $3d^{-1}$ hole states. These experimental studies gave us a good understanding of the branching ratio (BR) of double to the total decay probability, however, we are still unaware of the relative probability of cascade and direct double decay. Up to now, no theoretical studies have been carried out for

the DDAD process to understand the decay mechanism for Kr $3d^{-1}$ hole levels. In order to fully understand the complete physical picture of the Auger decay process, there is a strong need for deep theoretical investigations including both single and DAD processes to elucidate complete decay pathways. Yet such detailed theoretical studies are very much lacking for the DDAD process. To the best of our knowledge, there is only one theoretical prediction on the DDAD probability of Kr $3d^{-1}$ which employed a shake-off (SO) mechanism [13], which strongly underestimated the double decay fraction (1.2%) into higher charged ions of Kr^{3+} compared with the experimental results [10–12]. Further theoretical work [11] increased this relative yield from 1.2% to 20% by including the CDAD process. The experimentally measured BR of ∼30% for the decay into triply charged states [7, 10, 11] still awaits theoretical interpretation.

In this work, we investigate the Auger decay of Kr $3d^{-1}$ hole levels and construct the complete Auger decay pathway including both the single and double processes. The detailed level-to-level and level-to-configuration rates were obtained by using a distorted wave approximation with large-scale configuration interaction (CI) being taken into account. Very recently, we developed a theoretical procedure for the treatment of DDAD process according to the two generally accepted mechanisms of knock-out (KO) and SO and applied it to the Auger decay of Ar $2p^{-1}$ hole states [14]. The effect of electron correlations plays a more important role in the Auger decay of Kr $3d^{-1}$ than that of Ar $2p^{-1}$ both in single and double processes. The relatively lower kinetic energies of Auger transitions and the heavier overlap of the wave functions of Kr than Ar make the results more sensitive to electron correlations. Detailed level-to-level single and double Auger rates were used to interpret the experimentally measured double probability into the triply charged ion. Comparisons were made with available experimental results and complete pathways were obtained for the Auger decay of Kr $3d^{-1}$ hole levels by including the DDAD process.

2. Theoretical method

The theoretical procedure for the single and double Auger processes can be found in a recent work [14], here we give additional details in the following. In the first order perturbation theory, the SAD rate reads as (atomic units used in the theoretical description) [15, 16]

$$A^1_{im} = 2|\langle\Psi^+_m|\sum_{i<j}^{N}\frac{1}{r_{ij}}|\Psi_i\rangle|^2 \tag{1}$$

where $|\psi_i\rangle$ is the wavefunction of the initial autoionizing level of an ion with charge q and $|\Psi^+_m\rangle$ is the wavefunction of the level of an ion with charge q+1 plus a continuum electron. The total energy $E = \varepsilon_i$ for the initial level and $E = \varepsilon^+_m + k^2_m/2$ for the intermediate level with k_m being the momentum of the Auger electron. The wavefunctions of the initial autoionizing state with N electrons are obtained by diagonalizing the relativistic Hamiltonian [15]:

$$H = \sum_{i=1}^{N} H_D(i) + \sum_{i<j}^{N}\frac{1}{r_{ij}} \tag{2}$$

where $H_D(i)$ is the single-electron Dirac Hamiltonian for the potential due to the nuclear charge. The basis states ϕ_j, which are referred to as configuration state functions (CSFs), are antisymmetric sums of the products of N one-electron Dirac spinors $\varphi_{n\kappa m}$

$$\varphi_{n\kappa m} = \frac{1}{r}\begin{pmatrix} P_{n\kappa}(r)\chi_{\kappa m}(\theta,\psi,\sigma) \\ \mathrm{i}Q_{n\kappa}(r)\chi_{-\kappa m}(\theta,\psi,\sigma)\end{pmatrix} \tag{3}$$

where $P_{n\kappa}(r)$ and $Q_{n\kappa}(r)$ are radial functions for the large and small components of the orbital, and $\chi_{\kappa m}(\theta,\psi,\sigma)$ is a two-component spherical spinor; n, κ and m are the principal, relativistic angular and magnetic quantum numbers of the orbital, respectively. The relativistic angular quantum number κ is linked with the non-relativistic (l) and total (j) angular quantum number by $\kappa = (l - j)(2j + 1)$. The large and small components, $P_{n\kappa}(r)$ and $Q_{n\kappa}(r)$, satisfy the coupled Dirac equation for a local central potential $V(r)$ in the standard Dirac–Fock–Slator method

$$\begin{aligned}\left(\frac{\mathrm{d}}{\mathrm{d}r}+\frac{\kappa}{r}\right)P_{n\kappa} &= \alpha\left(\varepsilon_{n\kappa} - V + \frac{2}{\alpha^2}\right)Q_{n\kappa} \\ \left(\frac{\mathrm{d}}{\mathrm{d}r}-\frac{\kappa}{r}\right)Q_{n\kappa} &= \alpha(-\varepsilon_{n\kappa}+V)P_{n\kappa},\end{aligned} \tag{4}$$

where α is the fine-structure constant and $\varepsilon_{n\kappa}$ is the energy eigenvalue of the radial orbital. The radial wavefunction equation can be solved by a standard self-consistent field method.

The local central potential $V(r)$ includes the contributions from the nuclear charge and the electron–electron interaction and their detailed expressions can be found in the work of Gu [15]. The self-consistent iteration for the optimized local central potential is carried out based on the average configuration generated by a specified configuration group, which should always be the lowest lying one. The standard jj coupling scheme is used in coupling the angular momenta of successive shells. Various orbitals are assumed to be orthonormal:

$$\int_0^\infty (P_{n\kappa}P_{n'\kappa} + Q_{n\kappa}Q_{n'\kappa})\,\mathrm{d}r = \delta_{nn'}. \tag{5}$$

The initial autoionizing state is approximated by a linear combination of CSFs with the same symmetry to take the effects of CI into account

$$\Psi_i(J\pi) = \sum_j^{n_c} a_j\phi_j(J\pi), \tag{6}$$

where n_c is the number of CSFs and a_j denotes the representation of the atomic state in this basis. As there are no correlation effects between states with different total orbital angular momentum and parity $J\pi$, therefore we only need to diagonalize the same $J\pi$ states separately. If we simultaneously diagonalize all $J\pi$ states, there is no mixing between states with different total orbital angular momentum J and parity π.

The wavefunction of $|\Psi^+_m\rangle$ is constructed by coupling that of the ion state of $(N - 1)$ electrons with that of a continuum electron:

$$|\Psi^+_m\rangle = \sum_\kappa |\Psi_m, \kappa; J_T M_T\rangle \tag{7}$$

where the intermediate state $|\Psi_m\rangle$ has one less electron than $|\Psi_i\rangle$, J_T is the total angular momentum when the intermediate level is coupled to the continuum orbital, M_T is the projection of the total angular momentum and κ is the relativistic angular quantum number of the free electron. The wavefunction of $|\Psi_m\rangle$ is derived by using the same method as that of the initial autoionizing state with one less electron for the ion. The continuum orbitals are obtained by solving the Dirac equations with the same local central potential as that for bound orbitals and is normalized so that the large component has an asymptotic amplitude of $\sqrt{k/\varepsilon}$, which reduces to $\sqrt{2/k}$ in the non-relativistic limit, or equivalently,

$$\int_0^\infty [P_{\varepsilon(r)}P_{\varepsilon'}(r) + Q_{\varepsilon(r)}Q_{\varepsilon'}(r)]\,\mathrm{d}r = \pi\delta(\varepsilon - \varepsilon'), \tag{8}$$

where ε and k are the kinetic energy and kinetic momentum of the orbital, P_ε and Q_ε are the large and small components of the continuum wavefunction. In solving the continuum wavefunction, the radial grid is divided into two regions. In the inner region, where the wavefunction is not oscillatory, or the oscillation period is large enough to contain a sufficient number of grid intervals, the standard Numerov method is used to integrate the equation outward. Beyond some point $r = r_c$, which depends on the energy and angular momentum of the continuum sought, the oscillation period of the wavefunction becomes too small for the direct integration to be accurate. At that point, we switch to a phase–amplitude method. The inner and outer solutions are matched at r_c by requiring the continuity of the radial wavefunction and its first derivative.

In the independent particle approximation, the amplitude of the DDAD is zero as the initial $|\psi_i\rangle$ and final wavefunctions $|\Psi_f^{2+}\rangle$ differ by more than two single-electron states. In this case, the matrix element $\langle\Psi_f^{2+}|\sum_{i<j}^{N}\frac{1}{r_{ij}}|\Psi_i\rangle$, determining the amplitude of the DDAD rate, is zero. Hence it is necessary to take the electron correlations into account for the calculation of the DDAD rate, which in the second-order perturbation theory reads as

$$A_{if}^2 = \frac{8}{\pi}\int_0^{k_{\max}}\frac{\mathrm{d}k_{f1}}{k_{f2}} \times \left|\sum_m \sum\!\!\!\!\!\!\int_{k_m} \frac{\langle\Psi_f^{2+}|\sum_{i<j}^{N}\frac{1}{r_{ij}}|\Psi_m^{+}\rangle\langle\Psi_m^{+}|\sum_{i<j}^{N}\frac{1}{r_{ij}}|\Psi_i\rangle}{\varepsilon_i - \varepsilon_m^{+} - k_m^2/2}\right|^2 \tag{9}$$

where $|\Psi_f^{2+}\rangle$ is the wavefunction of the final level of an ion with charge q+2 plus two continuum electrons. In this formula, the frozen-core approximation was assumed and in the present work the core of $1s^22s^22p^63s^23p^6$ was used to get the set of one-electron orbitals with which Kr^+, Kr^{2+} and Kr^{3+} ionic wavefunctions were built. The total energy $E = \varepsilon_f^{2+} + E_{\max}$ is conserved with that of the initial level $E = \varepsilon_i$, where $E_{\max} = k_{f1}^2/2 + k_{f2}^2/2$ with k_{f1} and k_{f2} being the momenta of two Auger electrons. The summations over the intermediate middle level $|\Psi_m^+\rangle$ in the double Auger rate include a summation over all possible (q+1) ion levels and a summation over a complete set of bound and continuum states of the remaining electron. The intermediate middle level summations are calculated by summing over a finite number of bound levels and then integrating over continuum states. Such calculations are complex and challenging. In order to simplify the computation, approximate formulas can be deduced according to two generally agreed mechanisms: SO and KO [17], which read as

$$A_{\mathrm{KO}}^2 = \sum_m A_{im}^1\Omega_{mf}(\varepsilon_0) \tag{10}$$

and

$$A_{\mathrm{SO}}^2 = \sum_m A_{im}^1\left|\langle\Psi_f^{2+}\left|\Psi_m\right\rangle\right|^2 \tag{11}$$

where A_{im}^1 is the SAD rate from the initial hole level i to a middle level m and $\Omega_{mf}(\varepsilon_0)$ is the collision strength of the inelastic scattering of the 'intermediate' Auger electron upon the middle level m to the final level f. Note that atomic units are used in the above expressions and the electron impact collision strength is dimensionless. The matrix element $|\langle\Psi_f^{2+}|\Psi_m\rangle|$ means the overlap integral between the two wave functions determined in the field of the middle level and in the field of vacancies with two Auger electrons being emitted. Its calculation is straightforward with one less electron in both wavefunctions.

In a previous work [14], we demonstrated that KO is the dominant DDAD mechanism for the Ar $2p^{-1}$ hole state, not only for the total rate but also for contributions from any channel to Ar^{3+}. Therefore, the interference effect between the KO and SO mechanisms is negligible. For the Auger decay of Kr $3d^{-1}$, however, new features appear. Firstly, the proportion of SO contribution is increased for the Auger decay of Kr $3d^{-1}$ hole levels. The rates for some channels are comparable for the KO and SO mechanisms, which means that a stronger interference effect might occur for these channels. Exploring such interference effects experimentally is important for a deeper understanding of the Auger decay processes. Secondly, CDAD plays a much more important role for Kr $3d^{-1}$ than Ar $2p^{-1}$. According to our calculations, the proportion of CDAD and DDAD rates is nearly equal for the decay of Kr $3d^{-1}$, while CDAD rates are much lower than DDAD rates for Ar $2p^{-1}$. The difference for the two hole states is due to the different electronic structures of the respective ions. Elucidating the roles of electronic correlation on the Auger decay processes is important and useful for further applications.

3. Results and discussion

The calculations were carried out by using FAC code developed by Gu [15] with proper modifications to obtain the DDAD rates. The details to obtain the wavefunctions with local central potential can be found in the work of Gu [15]. Here we describe the calculational details relevant to our work. As the DDAD process was entirely due to the effects of electron correlation, it is necessary to properly describe these effects. The CI effect plays a more important role for the decay of Kr $3d^{-1}$ than that of Ar $2p^{-1}$ [14]. Previous researches showed the importance of strong electron correlation in the Auger decay of Kr $3d^{-1}$ and the correlated satellites [18–21].

In order to adequately take this effect into account, large-scale CI calculations were carried out to obtain the single and DAD rates for the hole levels belonging to the configuration $[Ar]3d^9 4s^2 4p^6$ of Kr^+, where [Ar] means $1s^2 2s^2 2p^6 3s^2 3p^6$. The DDAD process concerns bound state wavefunctions of three different successive ionization stages, i.e., Kr^+, Kr^{2+} and Kr^{3+}, a balanced treatment of electron correlations for these ions is vital to properly describe such a process. Such a balance means that, on one hand, the wavefunctions of Kr^+, Kr^{2+} and Kr^{3+} ions should be as accurate as possible in a complete set of calculations, and on the other hand, the same scale of electron correlations should apply for all relevant ions. To fulfil the first requirement, we optimize the complexes of $([Ni])4s^x 4p^y$ ($x + y = 7$, 6 and 5 for Kr^+, Kr^{2+} and Kr^{3+}, respectively) of all three ions simultaneously. Explicitly, the local central potential and the wavefunctions of the orbitals of 1s, 2s, 2p, 3s, 3p, 3d, 4s and 4p are obtained by simultaneously optimizing the configurations of $4s^2 4p^5$ and $4s4p^6$ of Kr^+, $4s^2 4p^4$, $4s4p^5$ and $4s^0 4p^6$ of Kr^{2+} and $4s^2 4p^3$, $4s4p^4$ and $4s^0 4p^5$ of Kr^{3+}. In this way, the same set of wavefunctions are derived with reasonable accuracy for all three ions. In the present work, we derived the wavefunctions in such a method. Actually, this is not a 'must' as we calculate the DDAD rates according to the simplified approximations, where the wavefunctions of only two successive ions are connected. Therefore one can also optimize the wavefunctions of two successive ions separately to get a higher possible accuracy. In order to fulfil the second requirement, singly and doubly excitations from the respective ground configurations of the successive ionization stages (Kr^+, Kr^{2+} and Kr^{3+}) to orbitals of 4d, 4f, 5s, 5p and 5d are considered for the electron correlations. Taking Kr^+ as an example to illustrate the scale of CI, the interactions among the fine-structure levels belonging to the following configurations are included: $4s^2 4p^5$, $4s4p^6$, $4s^2 4p^4 nl$, $4s4p^5 nl$, $4s^0 4p^6 nl$, $4s^2 4p^3 4dnl$, $4s4p^4 4dnl$, $4s^0 4p^5 4dnl$, $([Ar])3d^9 4s^2 4p^6$, $3d^9 4s^2 4p^5 nl$, $3d^9 4s4p^6 nl$, $3d^9 4s^2 4p^4 4dnl$ and $3d^9 4s4p^5 4dnl$ (nl = 4d, 4f, 5s, 5p and 5d).

For Kr^{2+} and Kr^{3+}, the same criteria were used to include the electron correlation effects to ensure the same scale of CI. The wavefunctions of the excited orbitals of 4d, 4f, 5s, 5p and 5d were obtained in the same local central potential as in optimizing the complexes of the respective ions. In this work, we study the Auger decay of $3d^9 4s^2 4p^6$, the main channels are $4s^2 4p^4$, $4s4p^5$, $4s^0 4p^6$ and $4s^2 4p^3 4d$ for the SAD and $4s^2 4p^3$ and $4s4p^4$ for the double Auger processes. The inclusion of the above configurations can describe our investigated processes reasonably well. Previous work showed the roles of CI effects on the radiative properties of hot dense plasmas [22–25].

Table 1 shows the fine-structure level-to-level SAD rates of Kr $3d^{-1}$ for the strong decay channels with a rate larger than 1.0×10^{12} s^{-1}. From the inspection of table 1, one can see that the strongest channel originates from the level of $(4s_{1/2} 4p^2_{1/2} 4p^3_{3/2})_1$ for both levels of Kr $3d^{-1}_{5/2}$ and $3d^{-1}_{3/2}$, whose Auger decay rate are 2.155×10^{13} and 2.235×10^{13} s^{-1}, respectively. The next strongest channel is due to the level of $(4s^2(4p_{1/2}(4p^2_{3/2})_2)_{5/2} 4d_{5/2})_1$, which has an Auger decay rate of 1.719×10^{13} and 1.822×10^{13} s^{-1}, respectively. For these two channels, the rate of $3d^{-1}_{3/2}$ is a little higher than that of the $3d^{-1}_{5/2}$ level. The total Auger rate due to all possible channels is 1.367×10^{14} and 1.345×10^{14} s^{-1}, respectively, for the two levels of Kr $3d^{-1}_{5/2}$ and $3d^{-1}_{3/2}$. Adding up the rates to levels belonging to a particular configuration by summing over all possible levels of it, we obtained level-to-configuration rates and BRs to the dominant pathways, which are given in table 2. The three most important pathways are due to the configurations of $4s^3 4p^3 4d$, $4s4p^5$ and $4s^2 4p^4$, representing a BR of 26.3%, 24.7% and 16.8% for Kr $3d^{-1}_{5/2}$ and 26.1%, 23.9% and 17.8% for Kr $3d^{-1}_{3/2}$, respectively. The two levels show basically the same decay pattern and BR. The other channels of descending BRs originate from configurations of $4s^2 4p^2 4d^2$, $4p^6$, $4s^2 4p^2 4d5s$, $4s^2 4p^3 5s$, $4s^2 4p^3 5d$ and $4s4p^4 4d$.

Table 1. Fine-structure level-to-level SAD probability A^1 (s^{-1}) for the strong channels (larger than 1.0×10^{12} s^{-1}) of Kr $3d^{-1}$ hole states. Figures in brackets indicate powers of ten. Columns refer to the initial $3d^{-1}$ levels, middle state designations, angular momenta (J) and energies (in eV) of the middle states (relative to the ground level of Kr $4s^2 4p^5\ ^2P_{3/2}$), and the last two columns to the transition energies ΔE (in eV) and Auger decay rates.

Level	Middle level	J	Energy	ΔE	A^1
$3d^{-1}_{5/2}$	$4s^2 4p^2_{1/2} 4p^2_{3/2}$	2	23.99	56.10	3.252(12)
	$4s^2 4p_{1/2} 4p^3_{3/2}$	1	24.49	55.59	1.134(12)
	$4s^2 4p_{1/2} 4p^3_{3/2}$	2	26.03	54.06	1.310(13)
	$4s^2 4p^4_{3/2}$	0	28.19	51.90	4.672(12)
	$4s_{1/2} 4p^2_{1/2} 4p^3_{3/2}$	2	38.52	41.56	4.294(12)
	$4s_{1/2} 4p_{1/2} 4p^4_{3/2}$	1	38.90	41.18	5.878(12)
	$4s_{1/2} 4p_{1/2} 4p^4_{3/2}$	0	39.17	40.91	2.070(12)
	$4s^2(4p_{1/2}(4p^2_{3/2})_2)_{5/2} 4d_{5/2}$	1	41.89	38.20	1.729(13)
	$4s^2 4p^3_{3/2} 5s_{1/2}$	1	47.44	32.64	2.183(12)
	$4s^2(4p_{1/2}(4p^2_{3/2})_2)_{5/2} 4d_{5/2}$	2	47.85	32.23	1.172(12)
	$4s^2 4p^3_{3/2} 4d_{3/2}$	1	48.05	32.03	2.697(12)
	$4s_{1/2} 4p^2_{1/2} 4p^3_{3/2}$	1	49.37	30.72	2.155(13)
	$4s^2 4p^3_{3/2} 4d_{5/2}$	1	50.57	29.51	1.160(13)
	$4p^2_{1/2} 4p^4_{3/2}$	0	56.65	23.43	1.127(13)
	$4s^2((4p^2_{3/2})_2 4d_{5/2})_{1/2} 5s_{1/2}$	0	65.64	14.44	4.230(12)
	$4s^2(4p_{1/2} 4p_{3/2})_2(4d_{5/2})_2$	0	66.89	13.20	6.619(12)
	$4s^2(4p^2_{3/2})_2 4d_{5/2})_{1/2} 5s_{1/2}$	0	72.74	7.34	1.872(12)
	$4s^2((4p^2_{3/2})_2 4d_{3/2})_{5/2} 4d_{5/2}$	0	74.12	5.96	3.860(12)
	$4s^2(4p^2_{3/2})_2(4d^2_{5/2})_2$	0	75.63	4.46	1.602(12)
	All possible channels				1.367(14)
$3d^{-1}_{3/2}$	$4s^2 4p^2_{1/2} 4p^2_{3/2}$	2	23.99	57.36	1.231(12)
	$4s^2 4p_{1/2} 4p^3_{3/2}$	1	24.49	56.85	1.932(12)
	$4s^2 4p_{1/2} 4p^3_{3/2}$	2	26.03	55.32	1.423(13)
	$4s^2 4p^4_{3/2}$	0	28.19	53.16	6.226(12)
	$4s_{1/2} 4p^2_{1/2} 4p^3_{3/2}$	2	38.52	42.83	8.799(12)
	$4s^2(4p_{1/2}(4p^2_{3/2})_2)_{5/2} 4d_{5/2}$	1	41.89	39.46	1.822(13)
	$4s^2 4p^3_{3/2} 5s_{1/2}$	2	47.05	34.30	1.096(12)
	$4s^2 4p^3_{3/2} 5s_{1/2}$	1	47.44	33.90	1.620(12)
	$4s^2(4p_{1/2}(4p^2_{3/2})_2)_{5/2} 4d_{5/2}$	2	47.85	33.50	2.417(12)
	$4s_{1/2} 4p^2_{1/2} 4p^3_{3/2}$	1	49.37	31.98	2.235(13)
	$4s^2 4p^3_{3/2} 4d_{5/2}$	1	50.57	30.77	1.206(13)
	$4p^2_{1/2} 4p^4_{3/2}$	0	56.65	24.70	1.038(13)
	$4s^2((4p^2_{3/2})_2 4d_{5/2})_{1/2} 5s_{1/2}$	0	65.64	15.70	3.893(12)
	$4s^2(4p_{1/2} 4p_{3/2})_2(4d_{5/2})_2$	0	66.89	14.46	6.109(12)
	$4s^2((4p^2_{3/2})_2 4d_{5/2})_{1/2} 5s_{1/2}$	0	72.74	8.61	1.898(12)
	$4s^2((4p^2_{3/2})_2 4d_{3/2})_{5/2} 4d_{5/2}$	0	74.12	7.23	3.838(12)
	$4s^2(4p^2_{3/2})_2(4d^2_{5/2})_2$	0	75.63	5.72	1.626(12)
	All possible channels				1.345(14)

Table 2. SAD rates (s^{-1}) and BRs (in per cent %) of Kr $3d^{-1}$ to the dominant configurations of Kr^{2+}. Figures in brackets indicate powers of ten.

Level	Final config.	Rate	BR
$3d_{5/2}^{-1}$	$4s^24p^4$	2.291(13)	16.8
	$4s4p^5$	3.380(13)	24.7
	$4p^6$	1.127(13)	8.2
	$4s^24p^34d$	3.601(13)	26.3
	$4s^24p^35s$	3.080(12)	2.3
	$4s^24p^35d$	2.215(12)	1.6
	$4s4p^44d$	1.675(12)	1.2
	$4s^24p^24d^2$	1.499(13)	11.0
	$4s^24p^24d5s$	7.388(12)	5.4
	Total	1.367(14)	100.0
$3d_{3/2}^{-1}$	$4s^24p^4$	2.397(13)	17.8
	$4s4p^5$	3.215(13)	23.9
	$4p^6$	1.038(13)	7.7
	$4s^24p^34d$	3.518(13)	26.1
	$4s^24p^35s$	2.846(12)	2.1
	$4s^24p^35d$	2.183(12)	1.6
	$4s4p^44d$	1.518(12)	1.1
	$4s^24p^24d^2$	1.414(13)	10.5
	$4s^24p^24d5s$	7.325(12)	5.4
	$4s^24p^24d5d$	1.771(12)	1.3
	Total	1.345(14)	100.0

The behaviour of the Auger decay pathways of Kr $3d^{-1}$ is rather different from that of Ar $2p^{-1}$. For the latter case, the dominant channels are due to the levels of $3s^23p^4$ and $3s3p^5$ configurations, which account for 75% and 12% of the total probability, respectively [14]. These two configurations represent a fraction of 87% in the total single decay process. For Kr $3d^{-1}$, however, the fraction due to the channels of $4s^24p^4$ and $4s4p^5$ configurations is only 41.5% of the total single decay probability, much smaller than that of Ar $2p^{-1}$ (87%). A considerable amount of the fraction is contributed by the higher excited configurations such as $4s^24p^34d$ and $4s^24p^24d^2$. Such a discrepancy is due to the different electron structure and correlations of the two initial hole states. For Kr $3d^{-1}$, the wave-function overlapping between initial levels and $4s^24p^34d$ is so strong that it has the largest decay probability to this configuration. However, such a wave-function overlapping is much smaller for Ar $2p^{-1}$, resulting in less probability to excited shells (such as $3s^23p^33d$). The energy of some of these excited levels is higher than the ionization potential of the doubly charged ion Kr^{2+}, resulting in a much higher cascade double Auger rate of Kr $3d^{-1}$ than that of Ar $2p^{-1}$.

The first ionization potentials of Kr^+ and Kr^{2+} are 24.36 and 35.97 eV, respectively, which means that the minimum energy to ionize Kr^+ to Kr^{3+} (the double ionization potential) is 60.33 eV [26]. From the inspection of table 1, one can see that the energy of channels such as $(4s^2((4p_{3/2}^2)_24d_{5/2})_{1/2}5s_{1/2})_0$, $(4s^2(4p_{1/2}4p_{3/2})_2(4d_{5/2})_2)_0$, $(4s^2(4p_{3/2}^2)_24d_{5/2})_{1/2}5s_{1/2})_0$, $(4s^2((4p_{3/2}^2)_24d_{3/2})_{5/2}4d_{5/2})_0$ and $(4s^2(4p_{3/2}^2)_2(4d_{5/2}^2)_2)_0$ is higher than 60.33 eV, meaning that these channels will further autoionize to the higher charged ion Kr^{3+}. The higher excited levels which show a strong Auger decay have a total angular momentum of zero. The energy of these channels is just slightly higher than the double ionization potential and therefore they dominantly autoionize to levels of the ground configuration $4s^24p^3$ of Kr^{3+}. To have a better understanding of the CDAD channels, we reformulate the Auger rates of the stronger pathways in table 3 for those levels whose energy lie above the first ionization potential. The dominant CDAD channels originate from the levels of configuration of $4s^24p^24d^2$, $4s^24p^24d5s$ and $4s4p^44d$, with total double cascade Auger rates of 2.693×10^{13} and 2.732×10^{13} s^{-1}, respectively, for the levels of Kr $3d_{5/2}^{-1}$ and $3d_{3/2}^{-1}$. If only CDAD pathways are considered in the DAD process, the double fraction into a triply charged ion is determined to be $2.693 \times 10^{13}/1.367 \times 10^{14} = 19.7\%$ and $2.732 \times 10^{13}/1.345 \times 10^{14} = 20.3\%$, respectively, for levels of Kr $3d_{5/2}^{-1}$ and $3d_{3/2}^{-1}$. The predicted fraction is in good agreement with the theoretical results obtained by Jonauskas *et al* [21], who derived a value of 20.0% and 19.8% for the levels of Kr $3d_{5/2}^{-1}$ and $3d_{3/2}^{-1}$, respectively. By using a relativistic CI method, these authors [21] showed that many-electron Auger transitions play an essential and even dominant role in the de-excitation of Kr $3d^{-1}$. Our theoretical results are in agreement with this statement. The average configuration value for the double decay fraction is 19.9% in our computation.

For a hole level, the natural lifetime width due to the single Auger process can be obtained by multiplying the Planck constant by the total decay rate and summing over all possible levels whose energy is lower than the hole level. The accuracy of the calculated SAD rates can be compared with the experimental lifetime [27, 28]. Jurvansuu *et al* [27] experimentally determined the natural widths of the shallow hole states of rare gases, including Kr $3d^{-1}$, from photoelectron spectra. The lifetime widths are obtained by fitting the photoelectron lines with pure Lorentzian line shapes. From the inspection of the measured photoelectron lines shown in the work of Jurvansuu *et al* [27], it can obviously be seen that the energy range of the photoelectron is very narrow around the resonance position. Drescher *et al* [28] measured a lifetime of $7.9^{+1.0}_{-0.9}$ femtoseconds (fs) by a pump-probe experiment combining a few-fs visible light pulse and a synchronized sub-fs soft x-ray pulse. Our calculated lifetime widths are compared with the experimental results [27, 28] in table 4. Good agreement is found between the theoretical and experimental results [27, 28]. The predicted level resolved and configuration-averaged lifetime widths are within the error bars of the experimental values. Note, however, that the DDAD process contributes to the natural widths as well.

Now we turn to the DDAD process. Table 5 shows some strong channels in the fine-structure levels contributed by the KO and SO mechanisms. For the KO mechanism, the contribution of the real part from the transition amplitude to the Auger decay rate is by far smaller than that of the imaginary part, just as demonstrated for the decay of Ar $2p^{-1}$ hole levels [14]. Hence we do not give the rates contributed by the real parts of the transition amplitudes. Such a conclusion verified that the decomposition of the KO mechanism is valid for Kr $3d^{-1}$. From the inspection of table 5, one can see that the rates contributed by the SO mechanism are much

Table 3. The same as table 1, but for those strong channels with a rate larger than 2.0×10^{11} s^{-1} which can DAD sequentially into a triply charged ion of Kr^{3+}.

Level	Middle level	J	Energy	ΔE	A^1
$3d_{5/2}^{-1}$	$(4s_{1/2}4p_{1/2}^2(4p_{3/2}^2)_2)_{3/2}4d_{3/2}$	0	61.81	18.27	2.043(11)
	$(4s_{1/2}4p_{1/2}^2(4p_{3/2}^2)_2)_{5/2}4d_{3/2}$	3	62.91	17.17	2.707(11)
	$4s^2((4p_{1/2}4p_{3/2})_14d_{3/2})_{1/2}5s_{1/2}$	0	65.41	14.67	2.561(11)
	$4s^2((4p_{3/2}^2)_24d_{5/2})_{1/2}5s_{1/2}$	0	65.64	14.44	4.230(12)
	$4s^24p_{1/2}^2(4d_{3/2}^2)_0$	0	66.42	13.67	2.152(11)
	$4s^2(4p_{1/2}4p_{3/2})_2(4d_{5/2}^2)_2$	0	66.89	13.20	6.619(12)
	$4s^2((4p_{3/2}^2)_14d_{3/2})_{5/2}4d_{5/2}$	0	67.34	12.74	5.696(11)
	$4s^2((4p_{1/2}4p_{3/2})_24d_{3/2})_{1/2}5s_{1/2}$	0	69.10	10.98	2.002(11)
	$4s^2((4p_{1/2}4p_{3/2})_2(4d_{5/2}^2)_2$	3	72.11	7.97	2.212(11)
	$4s^2((4p_{3/2}^2)_24d_{5/2})_{1/2}5s_{1/2}$	0	72.74	7.34	1.872(12)
	$4s^2((4p_{3/2}^2)_24d_{3/2})_{5/2}4d_{5/2}$	0	74.12	5.96	3.860(12)
	$4s^2(4p_{3/2}^2)_2(4d_{5/2}^2)_2$	0	75.63	4.46	1.602(12)
	All possible cascade channels				2.693(13)
$3d_{3/2}^{-1}$	$(((4s_{1/2}4p_{1/2})_14p_{3/2}^3)_{3/2})_{5/2}4d_{3/2}$	2	62.86	18.48	2.049(11)
	$4s^2((4p_{1/2}4p_{3/2})_14d_{3/2})_{1/2}5s_{1/2}$	0	65.41	15.94	2.548(11)
	$4s^2((4p_{3/2}^2)_24d_{5/2})_{1/2}5s_{1/2}$	0	65.64	15.70	3.893(12)
	$4s^24p_{1/2}^2(4d_{3/2}^2)_0$	0	66.42	14.93	3.299(11)
	$4s^2(4p_{1/2}4p_{3/2})_2(4d_{5/2}^2)_2$	0	66.89	14.46	6.109(12)
	$4s^2((4p_{3/2}^2)_14d_{3/2})_{5/2}4d_{5/2}$	0	67.34	14.01	5.908(11)
	$4s^2((4p_{1/2}4p_{3/2})_24d_{3/2})_{1/2}5s_{1/2}$	0	69.10	12.24	3.663(11)
	$4s^2((4p_{3/2}^2)_24d_{5/2})_{1/2}5s_{1/2}$	0	72.74	8.61	1.898(12)
	$4s^2((4p_{3/2}^2)_24d_{3/2})_{5/2}4d_{5/2}$	0	74.12	7.23	3.838(12)
	$4s^2(4p_{3/2}^2)_2(4d_{5/2}^2)_2$	0	75.63	5.72	1.626(12)
	$4s^2((4p_{3/2}^2)_24d_{5/2})_{5/2}5d_{5/2}$	0	80.72	0.63	2.232(11)
	$4p_{1/2}^24p_{3/2}^34d_{5/2}$	1	81.18	0.17	3.020(11)
	All possible cascade channels				2.732(13)

Table 4. Comparison of our theoretical lifetime widths (meV) of the Kr $3d^{-1}$ hole states due to the SAD processes with the experimental values from the literature, with the errors given in parentheses. Numbers in square brackets refer to the sources of the literature from which values are taken.

Level	This work	Expt.
$3d_{5/2}^{-1}$	90.0	88(4) [27]
$3d_{3/2}^{-1}$	88.6	88(4) [27]
$3d^{-1}$	89.4	$83.3^{+10.7}_{-9.3}$ [28]

smaller than that of KO mechanism for most channels, yet the contributions from the levels of $(4s^24p_{1/2}(4p_{3/2}^2)_2)_{3/2}$ and $((4s_{1/2}4p_{1/2})_04p_{3/2}^3)_{3/2}$ to the rates are comparable for the two mechanisms. This means that the effect of CI plays a more important role for the DDAD of Kr $3d^{-1}$ than that of Ar $2p^{-1}$ hole levels. The strong CI effect results in a strong overlapping of the wavefunctions for some particular channels and thus gives rise to a challenge for the accurate treatment of the DDAD process. For channels with comparable KO and SO rates, the interference effect between the KO and SO mechanisms might play a role. In total, the DDAD rate contributed by the KO mechanism is 2.046×10^{13} and 2.202×10^{13} s^{-1} for Kr $3d_{5/2}^{-1}$ and $3d_{3/2}^{-1}$, respectively, which are much larger than the corresponding values of 5.671×10^{12} and 5.938×10^{12} s^{-1} due to the SO mechanism.

The Auger decay electron spectra of Kr $3d^{-1}$ are summarized in figure 1, with plots 1(a) and (b) referring to the SAD process and plots 1(c) and (d) to the DDAD process for Kr $3d_{5/2}^{-1}$ and $3d_{3/2}^{-1}$, respectively. It is obtained by including the lifetime broadening and an assumed instrument resolution of 0.5 eV by using a Voigt profile

$$I(E) = A\frac{\sqrt{ln2}}{\sqrt{\pi}\Gamma_g}H(a, v) \tag{12}$$

where $I(E)$ is the intensity of single or double Auger electrons at energy E which is the energy of an Auger electron for SAD and the sum of two Auger electrons for the DDAD, A refers to the single A^1 or double A^2 rates which are obtained according to the above method and $H(a, v)$ is the Voigt function. Note that for the DDAD process the sum of the energy for the two Auger electrons is used as the functional variable E. For strongly asymmetric energy distribution for the two ejected electrons, it approximately is the intensity distribution of the fast ejected electron. From the inspection of figure 1, one can see that the energy of some channels pertaining to the same configuration are so close that they coalesce together both for the single and direct double decay. In figures 1(a) and (b), the Auger transitions located at 50–60 eV decay to the ground configuration $4s^24p^4$ of Kr^{2+} and the strong structures at 30–50 eV to configurations of $4s4p^5$ and $4s^24p^34d$ of Kr^{2+}. From the energy conservation law, we know that the Auger transitions below 20 eV in figures 1(a) and (b) belong to the CDAD process, which will further decay to a triply charged ion with dominant channels to the ground configuration $4s^24p^3$ of Kr^{3+}. The DDAD transitions shown in figures 1(c) and (d) decay to the ground configuration $4s^24p^3$ of Kr^{3+} for the structures above 15 eV, while those below 15 eV decay to

Table 5. Level-to-level DDAD rates (s^{-1}) for the dominant channels of Kr $3d^{-1}$ hole levels. The transition energy ΔE and the contributions from the KO and SO mechanisms are given in the last three columns. Figures in brackets indicate powers of ten.

Level	Final level	J	ΔE	A^2_{KO}	A^2_{SO}
$3d^{-1}_{5/2}$	$4s^24p_{1/2}(4p^2_{3/2})_2$	3/2	22.40	4.516(11)	3.527(11)
	$4s^24p^2_{1/2}4p_{3/2}$	3/2	19.91	2.369(12)	4.673(11)
	$4s^24p_{1/2}(4p^2_{3/2})_2$	5/2	19.74	3.874(12)	1.885(12)
	$4s^24p_{1/2}(4p^2_{3/2})_0$	1/2	18.32	1.356(12)	3.239(11)
	$4s^24p^3_{3/2}$	3/2	18.01	3.548(12)	1.941(12)
	$4s_{1/2}4p^2_{1/2}(4p^2_{3/2})_2$	5/2	7.60	1.043(12)	1.935(10)
	$(4s_{1/2}4p_{1/2})_04p^3_{3/2}$	3/2	7.21	5.046(11)	5.374(11)
	$4s_{1/2}4p^4_{3/2}$	1/2	6.98	1.487(11)	1.967(10)
	$(4s_{1/2}4p_{1/2})_14p^3_{3/2}$	3/2	3.66	2.096(12)	5.337(10)
	$(4s_{1/2}4p_{1/2})_14p^3_{3/2}$	5/2	3.54	3.100(12)	1.389(10)
	$4s^2(4p_{1/2}4p_{3/2})_14d_{3/2}$	3/2	1.70	1.470(11)	3.360(10)
	$4s^2(4p^2_{3/2})_24d_{5/2}$	1/2	1.35	2.377(11)	9.501(9)
	$4s^24p^2_{1/2}4d_{3/2}$	3/2	1.10	3.997(11)	2.242(9)
	$4s_{1/2}4p^2_{1/2}(4p^2_{3/2})_0$	1/2	0.35	8.597(11)	1.340(9)
	$4s^2(4p_{1/2}4p_{3/2})_14d_{3/2}$	1/2	0.17	1.147(11)	2.368(8)
	All possible levels			2.046(13)	5.671(12)
$3d^{-1}_{3/2}$	$4s^24p_{1/2}(4p^2_{3/2})_2$	3/2	23.67	4.150(11)	3.964(11)
	$4s^24p^2_{1/2}4p_{3/2}$	3/2	21.17	2.394(12)	4.172(11)
	$4s^24p_{1/2}(4p^2_{3/2})_2$	5/2	21.00	3.732(12)	1.773(12)
	$4s^24p_{1/2}(4p^2_{3/2})_0$	1/2	19.58	1.380(12)	3.411(11)
	$4s^24p^3_{3/2}$	3/2	19.28	3.621(12)	1.853(12)
	$4s_{1/2}4p^2_{1/2}(4p^2_{3/2})_2$	5/2	8.86	1.194(12)	3.201(10)
	$(4s_{1/2}4p_{1/2})_04p^3_{3/2}$	3/2	8.48	5.370(11)	5.950(11)
	$4s_{1/2}4p^4_{3/2}$	1/2	8.24	1.299(11)	2.866(10)
	$(4s_{1/2}4p_{1/2})_14p^3_{3/2}$	3/2	4.93	2.208(12)	1.514(11)
	$(4s_{1/2}4p_{1/2})_14p^3_{3/2}$	5/2	4.80	3.575(12)	4.398(10)
	$4s^2(4p_{1/2}4p_{3/2})_14d_{3/2}$	3/2	2.97	2.390(11)	6.743(10)
	$4s^2(4p^2_{3/2})_24d_{5/2}$	1/2	2.61	1.727(11)	1.124(10)
	$4s^24p^2_{1/2}4d_{3/2}$	3/2	2.37	3.007(11)	8.502(9)
	$4s_{1/2}4p^2_{1/2}(4p^2_{3/2})_0$	1/2	1.62	5.413(11)	1.278(10)
	$4s^2(4p_{1/2}4p_{3/2})_14d_{3/2}$	1/2	1.43	1.410(11)	1.400(9)
	$4s^2(4p^2_{3/2})_24d_{5/2}$	7/2	0.64	1.035(12)	9.320(10)
	All possible levels			2.202(13)	5.938(12)

the lowest two excited configurations of $4s4p^4$ and $4s^24p^24d$. The DDAD rates and BRs due to KO and SO mechanisms to the dominant configurations of Kr^{3+} are given in table 6. Both levels of $3d^{-1}_{5/2}$ and $3d^{-1}_{3/2}$ predominantly decay to the configurations of $4s^24p^3$ and $4s4p^4$. The total BR to these two configurations is 63.5% and 32.1% for $3d^{-1}_{5/2}$ and 58.4% and 32.4% for $3d^{-1}_{3/2}$. The Auger decay shows different trends for Kr $3d^{-1}$ and Ar $2p^{-1}$ [14], both for the SAD and DDAD processes. The rates and BRs are nearly the same for the two levels of Ar $2p^{-1}_{3/2}$ and $2p^{-1}_{1/2}$, while asymmetry increases evidently for Kr $3d^{-1}_{5/2}$ and $3d^{-1}_{3/2}$. The energy of the Auger electron(s) of Kr $3d^{-1}$ decay is much lower than that of Ar $2p^{-1}$. Moreover, the CDAD fraction of Kr $3d^{-1}$ decay is much higher than that of Ar $2p^{-1}$, showing more complex atomic structure and stronger CI of Kr.

Experiments using coincidence techniques measured the fraction of the DAD relative to the total rates for the decay of Kr $3d^{-1}$ into a triply charged ion [10, 29–31]. Present level-to-level single and DDAD rates can be used to interpret the experimental results. In table 7 we compared

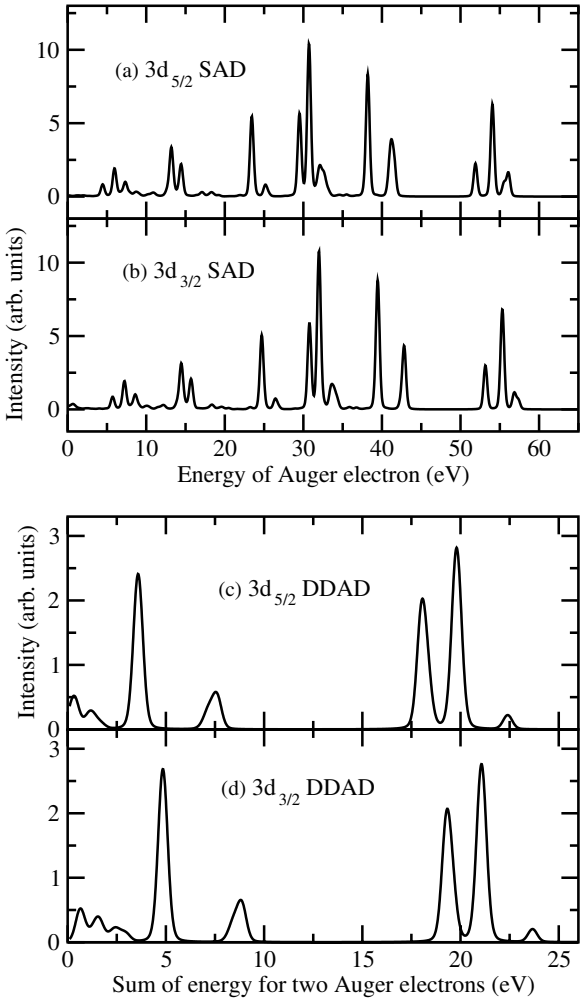

Figure 1. Auger electron spectra for SAD with CDAD of Kr (a) $3d^{-1}_{5/2}$, (b) $3d^{-1}_{3/2}$, and DDAD of (c) $3d^{-1}_{5/2}$ and (d) $3d^{-1}_{3/2}$.

our theoretical BR of a triply charged ion to the total yield with the observed values [10, 29–31]. Tamenori *et al* [29] experimentally observed a BR of 32(4)% for the decay into triply charged states by using monochromatized synchrotron radiation combined with a coincidence technique. The number in parenthesis shows the error in the last significant digit. Brunken *et al* [10] measured the level resolved fractions of 29(1)% and 31(1)% for Kr $3d^{-1}_{5/2}$ and $3d^{-1}_{3/2}$, respectively. Considering the contribution from only the KO mechanism, we obtained DDAD BRs of 12.6% and 13.6%, respectively, for the Kr $3d^{-1}_{5/2}$ and $3d^{-1}_{3/2}$, while the corresponding values are 16.1% and 17.2% including contributions from both KO and SO mechanisms. The double fraction due to the CDAD process is 16.5% and 16.8%, respectively, for the Kr $3d^{-1}_{5/2}$ and $3d^{-1}_{3/2}$, resulting in a total double BR of 29.1% and 30.4% by including only the KO mechanism and 32.6% and 34.0% when including both KO and SO mechanisms. The level resolved total double BRs of 32.6% and 34.0% are close to the experimental results of 29(1)% and 31(1)% [10] yet a little outside the error bars. The average configuration values of the total double BR for Kr $3d^{-1}$ are 29.6% and 33.2%, respectively, when considering only KO and both KO and SO mechanisms, which are in good agreement with the experimental value of 32(4)% obtained by

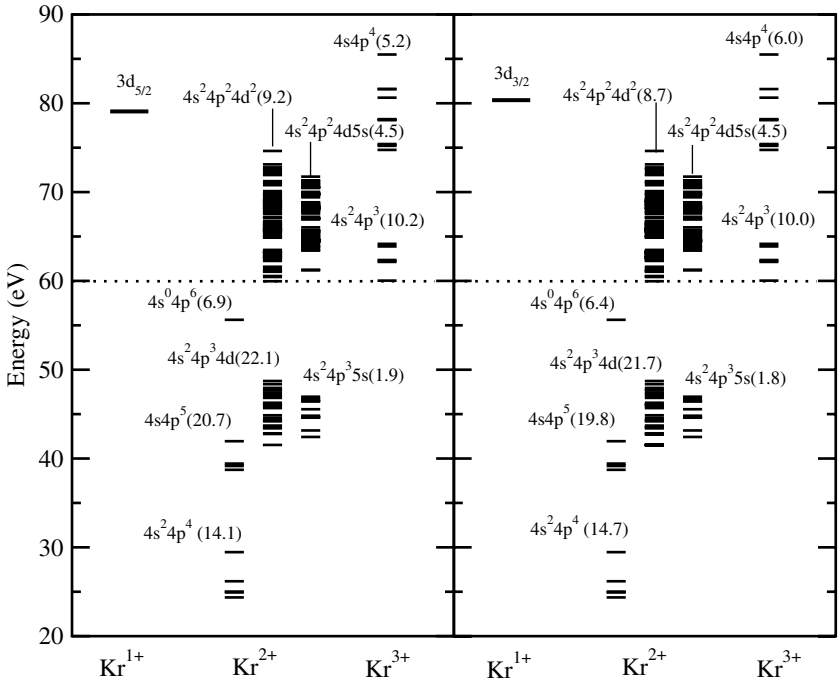

Figure 2. Pathways for the Auger decay (with a BR larger than 1.0%) of Kr (a) $3d_{5/2}^{-1}$ and (b) $3d_{3/2}^{-1}$ including the DDAD process. The number in the parenthesis after each configuration denotes the BR percentage for given configurations in %.

Table 6. The DDAD rates (s^{-1}) and BRs (in per cent %) of Kr $3d^{-1}$ to the dominant configurations of Kr^{3+}. Figures in brackets indicate powers of ten.

Level	Final config.	A^2_{KO}	KO BR	A^2_{SO}	SO BR	Total A^2	Total BR
$3d_{5/2}^{-1}$	$4s^24p^3$	1.160(13)	56.7	4.970(12)	87.7	1.657(13)	63.4
	$4s4p^4$	7.751(12)	37.9	6.450(11)	11.4	8.396(12)	32.1
	$4s^24p^24d$	1.110(12)	5.4	5.523(10)	1.0	1.165(12)	4.5
	Total	2.046(13)	100.0	5.671(12)	100.0	2.613(13)	100.0
$3d_{3/2}^{-1}$	$4s^24p^3$	1.154(13)	52.4	4.781(12)	80.5	1.632(13)	58.4
	$4s4p^4$	8.185(12)	37.2	8.638(11)	14.5	9.679(12)	32.4
	$4s^24p^24d$	2.290(12)	10.4	2.934(11)	4.9	2.583(12)	9.2
	Total	2.202(13)	100.0	5.938(12)	100.0	2.796(13)	100.0

Table 7. BRs (in per cent %) for the direct and CDAD of Kr $3d^{-1}$ and comparison of total theoretical double decay BRs with available experimental values in the literature. The numbers in parentheses for the experimental values show the errors in the last significant digit.

Level	DDAD BR (%)	CDAD BR (%)	Total BR (%)	Expt. (%)	Other theory (%)
$3d_{5/2}^{-1}$	12.6[a], 16.1[b]	16.5	29.1[a], 32.6[b]	29(1) [10]	20.0 [28]
$3d_{3/2}^{-1}$	13.6[a], 17.2[b]	16.8	30.4[a], 34.0[b]	31(1) [10]	19.8 [28]
$3d^{-1}$	13.0[a], 16.5[b]	16.6	29.6[a], 33.2[b]	32(4) [29], 30(1) [10] 26 [30], 25 [31]	1.2 [13]

Tamenori *et al* [29]. Earlier experimental results on the double BR of 26% determined by Saito and Suzuki [30] and 25% by Murakami *et al* [31] are lower than the later experimental values, which should be more accurate.

Previous theoretical work underestimated the double BR of Kr $3d^{-1}$. Jonauskas *et al* [21] predicted BRs of 20.0% and 19.8% for the levels of Kr $3d_{5/2}^{-1}$ and $3d_{3/2}^{-1}$, respectively, by considering the cascade double Auger process. The only theoretical prediction by including a SO mechanism available in the literature carried out by Kochur *et al* [13] obtained a value of 1.2% by using a straightforward Hartree–Fock model. Our work represents a theoretical work for the DDAD decay process of Kr inner-shell hole states by including both the KO and SO mechanisms. The results showed that KO is the dominant DDAD mechanism.

The complete Auger decay pathways of Kr $3d^{-1}$ hole states are summarized as follows:

$$\mathrm{Kr}^+\left(3d_{5/2}^{-1}\right) \overset{67.4\%}{\rightarrow} \mathrm{Kr}^{2+} \quad \text{via SAD} \quad \overset{16.5\%}{\rightarrow} \mathrm{Kr}^{3+} \quad \text{via CDAD}$$

$$\mathrm{Kr}^+\left(3d_{5/2}^{-1}\right) \qquad\qquad\qquad\quad \overset{16.1\%}{\rightarrow} \mathrm{Kr}^{3+} \quad \text{via DDAD}$$

$$\mathrm{Kr}^+\left(3d_{3/2}^{-1}\right) \overset{66.0\%}{\rightarrow} \mathrm{Kr}^{2+} \quad \text{via SAD} \quad \overset{16.8\%}{\rightarrow} \mathrm{Kr}^{3+} \quad \text{via CDAD}$$

$$\mathrm{Kr}^+\left(3d_{3/2}^{-1}\right) \qquad\qquad\qquad\quad \overset{17.2\%}{\rightarrow} \mathrm{Kr}^{3+} \quad \text{via DDAD.}$$

For the level of $3d_{5/2}^{-1}$, a fraction of 67.4% is predicted into Kr^{2+} via SAD and 16.5% and 16.1% into the triply charged ion Kr^{3+} via CDAD and DDAD processes, respectively. For the level of $3d_{3/2}^{-1}$, a fraction of 66.0% is predicted into Kr^{2+} via SAD and 16.8% and 17.2% into the triply charged ion Kr^{3+} via CDAD and DDAD processes, respectively. The theoretical results for the pathways including DDAD process are summarized in figure 2. The numbers in parentheses after each configuration denotes the BR percentage for a given configuration in %. The dotted line represents the position of the double ionization potential. Levels of Kr^{2+} below the dotted line belong to SAD channels, while above it belong to CDAD channels which can further decay to the levels of the ground configuration of Kr^{3+}. The results indicated that the fraction (16.6%) of CDAD of Kr $3d^{-1}$ is dramatically increased compared with that of Ar $2p^{-1}$ (2.9%), yet the fraction (16.5%) of DDAD is only slightly enhanced with the increase of atomic number. As a result, the total BR of DAD is evidently enhanced and is about twice of that of Ar $2p^{-1}$.

4. Conclusion

In conclusion, distorted wave calculations were carried out to investigate both the single and double Auger decay (DAD) rates of Kr $3d^{-1}$ hole states in the framework of the first and second perturbation theory. For the DDAD process, the complex transition amplitude is decomposed into approximate formulas according to two generally agreed mechanisms of knock-out (KO) and shake-off (SO). The results showed that the KO mechanism dominates in the DDAD process. The most important DDAD channels are due to the levels of configurations $4s^24p^3$ and $4s4p^4$, accounting for 63.5% and 32.1%, respectively, to the total double probability for Kr $3d_{5/2}^{-1}$ and 58.4% and 32.4% for Kr $3d_{3/2}^{-1}$. The total DDAD branching ratios (BRs) are 16.1% and 17.2%, respectively, for the two levels of Kr $3d_{5/2}^{-1}$ and $3d_{3/2}^{-1}$. By considering contributions from both single and double processes, the total double BRs including CDAD and DDAD are determined to be 32.6% and 34.0%, respectively, for levels of $3d_{5/2}^{-1}$ and $3d_{3/2}^{-1}$, resulting in an averaged configuration double probability of 33.2% into a triply charged ion. Our theoretical results were compared with the available experimental results on the BR into a triply charged ion and the results are within the error bars of the latest experimental measurement. An earlier theoretical work predicted a BR of 1.2% by using a SO mechanism, which strongly underestimated the decay probability into triply charged ions. The complete pathways were obtained by including the SAD with CDAD and DDAD processes. Compared with the Auger decay of Ar $2p^{-1}$, the fraction of the cascade double of Kr $3d^{-1}$ is dramatically enhanced yet that of direct double is only slightly increased. The total BR of DAD is about twice of that of Ar $2p^{-1}$.

Acknowledgments

This work was supported by the National Natural Science Foundation of China under grant numbers 11274382, 11274383 and 11204376. Calculations were carried out at the Research Center of Supercomputing Application, NUDT.

References

[1] Ackermann W *et al* 2007 *Nature Photon.* **1** 336
[2] Emma P *et al* 2010 *Nature Photon.* **4** 641
[3] Young L *et al* 2010 *Nature* **466** 56
[4] Vinko S M *et al* 2012 *Nature* **482** 59
[5] Xiang W, Gao C, Fu Y, Zeng J and Yuan J 2012 *Phys. Rev.* A **86** 061401
[6] Alkemper U, Doppelfeld J and von Busch F 1997 *Phys. Rev.* A **56** 2741
[7] Viefhaus J *et al* 2004 *Phys. Rev. Lett.* **92** 083001
[8] Penent F, Palaudoux J, Lablanquie P, Andric L, Feifel R and Eland J H D 2005 *Phys. Rev. Lett.* **95** 083002
[9] Nakano M *et al* 2012 *Phys. Rev.* A **85** 043405
[10] Brünken S, Gerth Ch, Kanngießer B, Luhmann T, Richter M and Zimmermann P 2002 *Phys. Rev.* A **65** 042708
[11] Palaudoux J *et al* 2010 *Phys. Rev.* A **82** 043419
[12] Andersson E *et al* 2010 *Phys. Rev.* A **82** 043418
[13] Kochur A G, Sukhorukov V L, Dudenko A I and Demekhin Ph V 1995 *J. Phys. B: At. Mol. Opt. Phys.* **28** 387
[14] Zeng J, Liu P, Xiang W and Yuan J 2013 *Phys. Rev.* A **87** 033419
[15] Gu M F 2008 *Can. J. Phys.* **86** 675
[16] Pindzola M S and Griffin D C 1987 *Phys. Rev.* A **36** 2628
[17] Amusia M Ya, Lee I S and Kilin V A 1992 *Phys. Rev.* A **45** 4576
[18] Aksela H, Aksela S and Pulkkinen H 1984 *Phys. Rev.* A **30** 2456
[19] Jauhiainen J, Aksela H, Aksela S, Kivimaki A, Sairanen O-P, Nommiste E and Vegh J 1995 *J. Phys. B: At. Mol. Phys.* **28** 3831
[20] Partanen L, Huttula M, Aksela H and Aksela S 2007 *J. Phys. B: At. Mol. Phys.* **40** 3795
[21] Jonauskas V, Karazija R and Kučas S 2008 *J. Phys. B: At. Mol. Phys.* **41** 215005
[22] Zeng J and Yuan J 2006 *Phys. Rev.* E **74** 025401
[23] Zeng J and Yuan J 2007 *Phys. Rev.* E **76** 026401
[24] Zeng J 2008 *J. Phys. B: At. Mol. Phys.* **41** 125702
[25] Zeng J and Yuan J 2002 *Phys. Rev.* E **66** 016401
[26] http://physics.nist.gov/cgi-bin/ASD/energy1.pl
[27] Jurvansuu M, Kivimaki A and Aksela S 2001 *Phys. Rev.* A **64** 012502
[28] Drescher M, Hentschel M, Klenberger R, Uiberacker M, Yakovev V, Scrinzi A, Westerwalbesloh Th, Kleineberg U, Heinzmann U and Krausz F 2002 *Nature* **419** 803
[29] Tamenori Y, Okada K, Tanimoto S, Ibuki T, Nagaoka S, Fujii A, Haga Y and Suzuki I H 2004 *J. Phys. B: At. Mol. Opt. Phys.* **37** 117
[30] Saito N and Suzuki I H 1997 *J. Phys. Soc. Japan* **66** 1979
[31] Murakami E, Hayaishi T, Yagishita A and Morioka Y 1990 *Phys. Scr.* **41** 468